Annihilation of vortex lines in rotating superfluid ^{3}He

V. M. Ruutu, J. J. Ruohio, and M. Krusius

Low Temperature Laboratory, Helsinki University of Technology, Box 2200, FIN-02015 HUT, Finland

B. Plaçais

Laboratoire de Physique de la Matière Condensée, École Normale Supérieure, CNRS URA 1437, F-75 231 Paris Cédex 05, France

E. B. Sonin* and Wen Xu

Low Temperature Laboratory, Helsinki University of Technology, Box 2200, FIN-02015 HUT, Finland

(Received 16 December 1996; revised manuscript received 22 May 1997)

In decelerating rotation, vortex lines annihilate in single-vortex events at the annihilation threshold where their number $N_{max}(\Omega)$ is equal to or exceeds the equilibrium value $N_{eq}(\Omega)$. A surplus $N_{max} - N_{eq}$ may be stabilized by an energy barrier, which during deceleration vanishes in an instability. We find the barrier to depend on container misalignment in ^{3}He-*B* and on the orbital texture in the container corners in ^{3}He-*A*. Measurements of the instability yield the circulation quantum of the vortex which is found to be consistent with the present identification of vortex structures in ^{3}He-*A*. [S0163-1829(97)02645-3]

In equilibrium a rotating superfluid is threaded by an array of rectilinear quantized vortex lines, which are parallel to the rotation axis $\boldsymbol{\Omega}$. If the rotation velocity Ω is slowly reduced, ultimately the peripheral lines will be pushed to the lateral walls (parallel to $\boldsymbol{\Omega}$) and annihilate there. What then is the largest possible number of lines $N_{max}(\Omega)$ which can be sustained in the container during decelerating rotation? Do the lines annihilate one by one or do they reach the wall in bunches of many lines? These questions have often been considered theoretically, but reliable experiments have been few. One reason is experimental resolution: Ideally to maintain a count of vortex lines, one needs single-vortex sensitivity. Also one needs to understand the mechanisms of vortex formation in detail. Here we report the first quantitative measurements on annihilation in rotating ^{3}He superfluids.

Rotating superfluid. The density of vortex lines in equilibrium rotation is $n_v = 2\Omega/\kappa$, where $\kappa = \nu h/2m_3$ is the circulation of a vortex with quantization number ν.[1] In the continuum limit a totally filled cylindrical container with radius R would have $N_0 = \pi R^2 n_v$ lines. Interactions with the lateral walls give rise to an annular vortex-free region along the wall.[2] Its width d is of order of the intervortex distance $r_v = (\kappa/2\pi\Omega)^{1/2}$ (expressed here as the radius of the Wigner-Seitz unit cell of the vortex lattice). As a result, the total line number $N(\Omega) \simeq N_0(1 - 2d/R)$ is always less than $N_0(\Omega)$.

Annihilation barrier. Rotating experiments are generally performed in a container whose lateral walls are meant to be parallel to the rotation axis $\boldsymbol{\Omega}$. Ideally in this geometry vortices do not connect to the lateral walls and annihilation is resisted by an energy barrier. It arises from the balance of two radial forces on the peripheral circle of rectilinear vortex lines: the inward directed Magnus force from the surrounding vortex-free counterflow and the attraction by the image vortex in the wall.[3] In ^{3}He superfluids energy barriers are generally large compared to temperature.[4] They cannot be overcome by thermal activation or quantum tunneling. Instead, during decelerating rotation the barrier ultimately vanishes because of the diminishing counterflow velocity. This

process, where the number of lines $N_{max}(\Omega)$ exceeds the equilibrium value $N_{eq}(\Omega)$, we call *intrinsic* annihilation at the annihilation instability. Deviations from the ideal parallel-wall geometry (i.e., a misalignment with respect to $\boldsymbol{\Omega}$ or a radius of curvature in the corners which exceeds r_v) may eliminate the annihilation barrier. In the presence of such *extrinsic* influence, $N(\Omega)$ equals at the annihilation threshold the line number in the equilibrium state: $N_{max}(\Omega) = N_{eq}(\Omega)$.

Annihilation threshold in ^{3}He-B. In Fig. 1 these principles are illustrated with measurements of $N_{max}(\Omega)$. The data have been recorded in a rotating nuclear demagnetization cryostat with NMR techniques and single-vortex resolution.[4] At high velocities, $\Omega > \Omega^\dagger \simeq 0.18$ rad/s, the annihilation threshold falls on the solid curve which represents the equilibrium
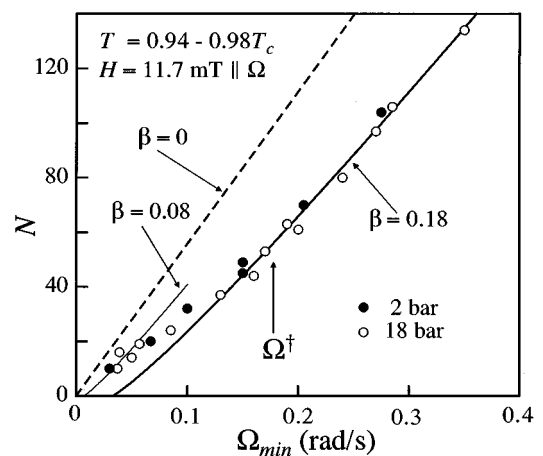

FIG. 1. Annihilation threshold of singular vortex lines in ^{3}He-*B*. The measured maximum line number N_{max} in the decelerated state is plotted as a function of Ω. The dashed line $N_0 = 560\Omega$ is the limit of solid body rotation, the thin solid curve $N_{inst} = N_0 - 2\sqrt{N_0}$ the annihilation instability, and the thick solid curve the equilibrium state $N_{eq} = N_0(1 - \beta/\sqrt{\Omega})$.
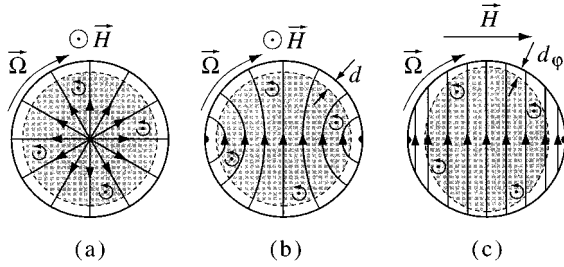
       <u>56</u>   14 089

FIG. 2. Planar $\hat{\mathbf{l}}(\mathbf{r})$ textures in a cylinder, when $H \gg H_D$. The lines denote the $\hat{\mathbf{l}}$ orientation in the transverse plane. The shaded area is the vortex array. (a) Radial disgyration texture, with one 2π vortex line in the center. (b) ''Double-half'' circular disgyration with two singular lines along the lateral walls. These two are possible equilibrium textures in an axially oriented magnetic field. (c) Pseudouniform texture in transverse field with a counterflow annulus of nonuniform width.

state. This identification has been established by comparison with the state which is created after a slow cool down through T_c at constant rotation. Here the vortex-free annulus[2,5] has the width $d = d_{\mathrm{eq}}(\Omega) = r_v[\frac{1}{2}\ln(r_v/r_c)]^{1/2}$, where $r_c \simeq \xi(T,P)$ (Ref. 6) is the vortex core radius and $\xi(T,P) \sim 0.1$–0.4 μm the superfluid coherence length in the temperature (T) and pressure (P) regime of our measurements. At the lowest velocities the data approach the thin line, the instability, where $d = d_{\mathrm{inst}} \simeq r_v$. Assuming that the crossover at $\Omega^{\dagger}$ arises from misalignment, one has $r_v(\Omega^{\dagger}) = L\sin\theta$, where L is the height of the container and θ the inclination between the cylinder and rotation axes.[7] The value $\Omega^{\dagger} \simeq 0.18$ rad/s corresponds to $\theta \simeq 2°$, which seems a realistic estimate of the experimental precision. $\Omega^{\dagger}$ is essentially independent of temperature and pressure.

Orbital anisotropy in ^{3}*He-A.* ^{3}He-*B* is a quasi-isotropic superfluid where vortices have a singular core and the annihilation properties are similar to those in ^{4}He II. In ^{3}He-*A*, vortices exist with both singular and continuous core structures, and also orbital anisotropy can be expected to influence annihilation. In Fig. 2 the equilibrium textures of the orbital unit vector $\hat{\mathbf{l}}$ are depicted in an infinitely long cylinder, when the external magnetic field H exceeds the dipolar field H_D ($\simeq 3.2$ mT). These $\hat{\mathbf{l}}(\mathbf{r})$ textures are smoothly varying, planar, and dipole locked over most of the cylindrical cross section (except at the topological lines), and are created in a slow cool down through T_c at constant rotation. We use this procedure to establish the initial state at $\Omega \simeq 0.6$ rad/s, from where deceleration to the annihilation threshold is started at constant T. During a slow deceleration $(|d\Omega/dt| < 10^{-3}$ rad/s$^2)$ the texture does not undergo a transition.

Two topologies with comparable energies are possible when the field is oriented along the cylinder axis: the radial disgyration ($\hat{\mathbf{l}} = \hat{\mathbf{r}}$), which has one central line along the axis [Fig. 2(a)], or the ''double-half'' circular disgyration with two singular lines at opposite sides of the circumference [Fig. 2(b)]. The transverse-field texture [Fig. 2(c)] has the same topology as the axial-field double-half disgyration, but its $\hat{\mathbf{l}}$ orientation is uniform. At the cylindrical wall $\hat{\mathbf{l}}$ is oriented along the surface normal within a surface layer with a width of order of the dipolar healing length $\xi_D \simeq 15\mu$m. It is not shown in Fig. 2(c).

Vortices in ^{3}*He-A.* In rotation rectilinear vortex lines are included in the $\hat{\mathbf{l}}(\mathbf{r})$ texture with no changes on the global scale. The vortices have a *soft vortex core* with radius $r_c \sim \xi_D$, within which the $\hat{\mathbf{l}}$ orientation becomes three-dimensional.[8] The circulation around a singularity-free soft core of a *continuous vortex* (CV) corresponds to two quanta: $\nu = 2$. A *singular vortex* (SV) has within its soft core also a singular ''hard core'' with a radius $\simeq \xi(T,P)$, in which the A-phase order parameter amplitude is depleted. The circulation of a SV is singly quantized: $\nu = 1$. The effective core radius $r_c = \xi_D e^{-\delta}$ depends weakly on the vortex structure: Numerical calculations in the Ginzburg-Landau regime yield $\delta_{\mathrm{CV}} \simeq -0.3$ and $\delta_{\mathrm{SV}} \simeq 2.1$.[9]

Annihilation instability in ^{3}*He-A.* The analysis of the annihilation barrier in Ref. 3 can be generalized to an anisotropic superfluid: In ^{3}He-*A* the superfluid density is a uniaxial tensor with eigenvalues $\rho_{\parallel}$ for flow parallel to $\hat{\mathbf{l}}$ and $\rho_{\perp}$ normal to $\hat{\mathbf{l}}$. The anisotropy ratio is $\gamma = \sqrt{\rho_{\perp}/\rho_{\parallel}}$ ($\simeq \sqrt{2}$). Inside the vortex-free region a single rectilinear line at a distance y from the wall has an energy per unit length given by

$$\epsilon_v(y) = \frac{\tilde{\rho}_s \kappa^2}{4\pi}\ln\frac{2y}{r_c} + \bar{\rho}_s\kappa\Omega(y^2 - 2dy). \quad (1)$$

The first term is the energy of the line in the fluid at rest, taking into account its image in the wall. The second term arises from the interaction of the velocity fields of the vortex and the vortex-free counterflow with the velocity $v(y) \simeq 2\Omega(y - d)$. This term is proportional to the total mass flow $\bar{\rho}_s\int v(y')dy'$ through the area between the line and the wall.[10] The effective density $\tilde{\rho}_s$ depends on the orientation of $\hat{\mathbf{l}}$ with respect to the local circular currents around a vortex while $\bar{\rho}_s(\phi)$ is the value in the direction of the counterflow and depends on the angle ϕ between the surface normal and $\hat{\mathbf{l}}$ in the bulk.

If one had $\hat{\mathbf{l}} \| \boldsymbol{\Omega}$, then the local superflow around the vortex core would be perpendicular to $\hat{\mathbf{l}}$, $\tilde{\rho}_s = \bar{\rho}_s = \rho_{\perp}$, and the streamlines would be circular. In the textures of Fig. 2, $\hat{\mathbf{l}}(\mathbf{r}) \perp \boldsymbol{\Omega}$, and the flow around the vortex core is elliptic. By rescaling one can make a transformation to circular stream lines. A calculation of the kinetic energy of the superflow around the soft core yields then an effective superfluid density $\tilde{\rho}_s = \sqrt{\rho_{\perp}\rho_{\parallel}}$.[11] One also finds that $\bar{\rho}_s(\phi) = \bar{\gamma}(\phi)\tilde{\rho}_s$, where the ϕ-dependent anisotropy ratio is $\bar{\gamma}(\phi) = [1 + (\gamma^2 - 1)\cos^2\phi]/\gamma$.

The equilibrium width of the vortex-free region is determined from the condition $\epsilon_v(y = d) \approx 0$. Then

$$d_{\mathrm{eq}}(\phi) = \left[\frac{1}{\bar{\gamma}(\phi)}\frac{\kappa}{4\pi\Omega}\ln\frac{r_v}{r_c}\right]^{1/2}. \quad (2)$$

Although the total mass counterflow $\propto \bar{\rho}_s d_{\mathrm{eq}}^2$ is constant within the vortex-free annulus also in the transverse-field texture of Fig. 2(c), $\bar{\rho}_s(\phi)$ and $d_{\mathrm{eq}}(\phi)$ are not. Equation (2) must be satisfied also for any metastable vortex-free region:

$d(\phi) \propto 1/\sqrt{\overline{\gamma}(\phi)}$. In the axial-field textures $\hat{\mathbf{l}}$ is radial in the vortex-free region [except close to the two singular lines in Fig. 2(b)]. As a result $\phi = 0$, $\overline{\rho}_s \equiv \rho_\perp$, and the vortex bundle is axisymmetric.

The derivative $d\epsilon_v/dy$ is the radial force on the vortex which vanishes at the two extrema of the energy profile,

$$y_\pm(\phi) = \frac{1}{2}[d \pm \sqrt{d^2 - r_v^2/\overline{\gamma}(\phi)}], \qquad (3)$$

where $r_v = \sqrt{\kappa/2\pi\Omega}$ is the ϕ-independent Wigner-Seitz radius. The energy profile $\epsilon_v(y)$ has a maximum at $y = y_-$ and a minimum at $y = y_+$, if $d\sqrt{\overline{\gamma}(\phi)} > r_v$. For $d\sqrt{\overline{\gamma}(\phi)} < r_v$, there are no extrema. At the annihilation instability the barrier height vanishes and

$$d_{\text{inst}}(\phi)\sqrt{\overline{\gamma}} \simeq r_v = \left[\frac{\kappa}{2\pi\Omega}\right]^{1/2}. \qquad (4)$$

In transverse field the positions $y_\pm$ of the extrema depend on ϕ, but the barrier vanishes homogeneously along the perimeter for $d(\phi)\sqrt{\overline{\gamma}} = r_v$, as in axial field. We therefore expect no difference between the annihilation thresholds $N_{\text{max}}(\Omega)$ of the three equilibrium $\hat{\mathbf{l}}(\mathbf{r})$ textures in Fig. 2. This result has been derived for the continuum limit with a well-defined border between the vortex-free annulus and the central vortex bundle: $d \gg r_v$. In the limit $d_{\text{inst}} \to r_v$, the width $d(\Omega)$ loses its transparent geometrical meaning, but can still be used to define approximately the deficit $N_0(\Omega) - N_{\text{max}}(\Omega)$.

Annihilation threshold of SVs in ^{3}He-A. In the A-phase NMR spectrum the vortex satellite peak is proportional to the vortex line number.[8] From the integrated satellite intensity I_{SV} normalized to the total resonance intensity I_{tot}, or $\mathcal{I}_{\text{SV}}(\Omega) = I_{\text{SV}}/I_{\text{tot}}$, we determine $N(\Omega)$ with an accuracy of ± 10 lines. The results fitted to the expression $\mathcal{I}_{\text{SV}} = \alpha(\Omega - \beta\sqrt{\Omega})$ yield $\beta = 2d\sqrt{\Omega}/R$, by analogy with $N(\Omega) = N_0(1 - 2d/R)$.

The results are plotted in Fig. 3 in the reduced form $\mathcal{I}_{\text{SV}}/\alpha$, for which no calibrations are needed. The data can be fit with $\alpha = 0.094 \pm 0.005, \beta = 0.08 \pm 0.03$ for the axial (open circle) and $\alpha = 0.136 \pm 0.005, \beta = 0.14 \pm 0.03$ for the transverse (solid circle) field orientations. The square data points denote the initial equilibrium states, obtained by cooling through T_c at 0.60 rad/s in the NMR field.[8] Their absorptions are equal and fall on the $\beta = 0.14$ curve. This value of β happens to agree exactly with $\beta = 0.18$ for the equilibrium state of ^{3}He-B in Fig. 1, bearing in mind the different r_c in Eq. (2). The axial-field fit in turn gives $\beta = 0.08$ which, when compared to Fig. 1 and Eq. (4), corresponds to that expected for the instability line in ^{3}He-A. Thus two smooth curves are obtained in Fig. 3 which bear no indication of a crossover feature at $\Omega^\dagger \sim 0.2$ rad/s, as was measured with the same experimental setup for ^{3}He-B.

Annihilation threshold of CVs in ^{3}He-A. The CV satellite peak in the NMR spectrum is shifted further from the large bulk liquid maximum than that of SVs and thus their number can be determined with a better resolution of ± 3 lines. In Fig. 4 their normalized intensity $\mathcal{I}_{\text{CV}}(\Omega)/\alpha$ has been plotted for measurements in both axial and transverse fields. There is again a large difference between their α values (axial field:
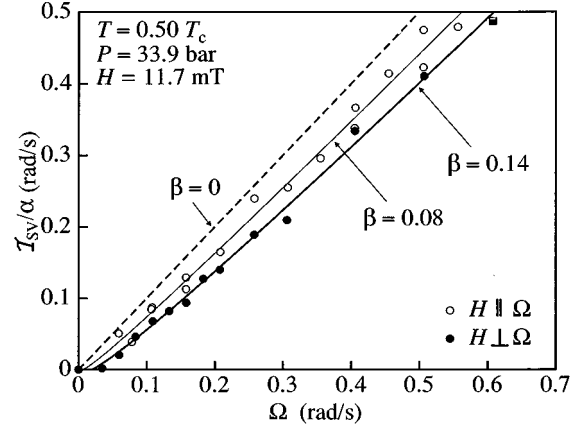

FIG. 3. Annihilation threshold of singular vortex lines in ^{3}He-A in axial ($\circ$) and transverse ($\bullet$) field, plotted as the normalized absorption $\mathcal{I}_{\text{SV}}/\alpha$. The thick and thin solid curves are fits which give $d = d_{\text{eq}}$ and $d = r_v$, respectively. The two data points marked with squares refer to the initial equilibrium states after cool down in rotation through T_c with the NMR field in axial ($\square$) or transverse ($\blacksquare$) orientations.

$\alpha = 0.114 \pm 0.003$; transverse field: $\alpha = 0.170 \pm 0.015$), but both sets of data give a good fit with $\beta = 0.16 \pm 0.01$. Inserting the appropriate κ and r_c into Eq. (2), we find that this result equals that expected for the equilibrium state and corresponds to $\beta = 0.18$ in ^{3}He-B.

During cool down through T_c at low Ω, CV lines are only formed at low fields,[8] $H < H_D$. Therefore the field was kept at zero during the cool down through T_c and was later swept up to the NMR value. In transverse field (solid square) the initial state lies on the $\beta = 0.16$ curve, as expected for the equilibrium state. Thus the transverse-field data repeat the behavior of Fig. 3: The annihilation threshold lies on the equilibrium curve and bears no evidence of the crossover feature of Fig. 1.
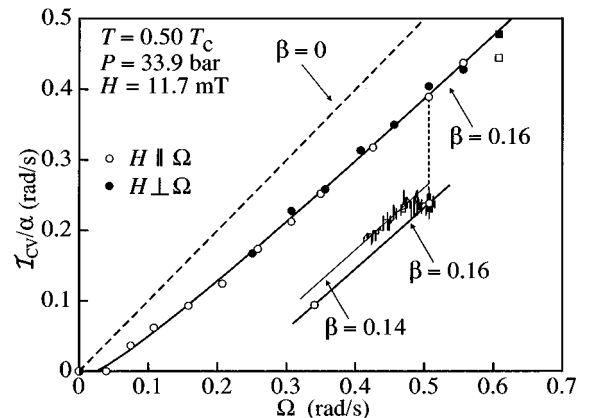

FIG. 4. Annihilation threshold of continuous vortex lines in axial ($\circ$) and transverse ($\bullet$) field, plotted as the normalized satellite absorption $\mathcal{I}_{\text{CV}}/\alpha$. The initial states, marked with square points, have been measured after a cool down through T_c at 0.60 rad/s in zero field and after sweeping the field up in axial ($\square$) and transverse ($\blacksquare$) orientations. The solid curve is a fit which gives $d = d_{\text{eq}}$. The inset shows a recording of the satellite peak height (scaled to $\mathcal{I}_{\text{CV}}/\alpha$), when deceleration is restarted after a long stop at constant $\Omega = 0.51$ rad/s.

However, the axial-field data in Fig. 4 display a slightly different pattern from those in Fig. 3: (1) The initial state (open square) supports approximately ten lines less than in transverse field. This deficit has to be attributed to a loss of lines while the field is increased to the NMR value. (2) The annihilation data fall on the same curve as in transverse field and not on one with a smaller β. (3) When decelerating to the annihilation threshold in axial field, a small but clearly distinguishable difference is observed in the CV satellite peak height, if it is measured at constant Ω or during continuous deceleration. Normally deceleration is stopped at some point, when the satellite amplitude is continuously decreasing and vortex lines are annihilating at a steady rate. The NMR spectrum is then recorded repeatedly at constant Ω over a period of 30 min. These data are plotted in Fig. 4 (open circle) and yield $\beta=0.16$. If deceleration is then resumed, as shown in the inset, the annihilation threshold is observed to have moved to a lower Ω value, corresponding to $\beta=0.14$, as expected for the annihilation instability. The difference between these two satellite heights corresponds to $\simeq 4$ lines at 0.5 rad/s. It is conceivable that it could arise from mechanical noise in the rotation drive while the NMR spectra are recorded during 30 min at constant Ω. However, this appears unlikely since this feature was only observed for CV lines in axial field.

Summary. Vortices annihilate smoothly and not in bunches, as has sometimes been suggested to explain the discontinuous glitches in neutron-star deceleration. Our measurements on the annihilation threshold in ^{3}He-*B*, expressed directly as vortex-line numbers, display for the first time the expected generic properties of an isotropic superfluid: At low Ω the line number N_{max} at the threshold exceeds the equilibrium value N_{eq} due to the presence of an energy barrier. At high Ω extrinsic effects remove the barrier and $N_{\mathrm{max}}=N_{\mathrm{eq}}$.

We showed that the equilibrium $\hat{\mathbf{l}}$ textures of ^{3}He-*A* in an infinitely long cylinder are not expected to influence annihilation: it should proceed as in the isotropic case. Nevertheless, differences from the generic behavior are observed, although they are small and comparable to our accuracy in $\mathcal{I}_{\mathrm{SV}}(\Omega)/\alpha_{\mathrm{SV}}$ and $\mathcal{I}_{\mathrm{CV}}(\Omega)/\alpha_{\mathrm{CV}}$. Indeed, the difference between d_{eq} and d_{inst} is roughly by a factor of 2 smaller for CV lines in the A phase, compared to the B phase. Still, the data on the annihilation threshold in ^{3}He-*A* give $d=d_{\mathrm{eq}}(\Omega)$ in transverse field, while axial-field data tend to suggest $d=d_{\mathrm{inst}}(\Omega)$. A crossover from one type of behavior to another is not found.

These observations point to the influence of the $\hat{\mathbf{l}}$ texture in the container corners where the barrier is smallest for the end of the vortex to bend and cross the vortex-free annulus. In axial field $\hat{\mathbf{l}}$ rotates in the corner within the plane which contains $\boldsymbol{\Omega}$ while in transverse field the texture is more complicated (ϕ dependent). Apparently, the transverse-field corner texture eliminates the barrier, but the axially symmetric axial-field corner texture enforces one, suppressing the effect from container misalignment.

Finally, the measurement of the annihilation instability gives the circulation κ, which we find to be consistent with the accepted view of the topologies of the vortex structures in ^{3}He-*A*. ^{3}He-*A* provides a model system for flux-line annihilation in anisotropic superconductors, where highly polished surfaces or cleaved crystals are required, together with an accurate alignment of the magnetic field, for the ''Bean-Livingston'' barrier to become observable.

---

*Permanent address: Ioffe Physical Technical Institute, St. Petersburg 194 021, Russia.

[1] R. J. Donnelly, *Quantized Vortices in Helium II* (Cambridge University Press, Cambridge, England, 1991).

[2] H. E. Hall, Adv. Phys. **9**, 89 (1960).

[3] P. Mathieu, J. C. Marechal, and Y. Simon, Phys. Rev. B **22**, 4293 (1980).

[4] V. M. Ruutu *et al.*, J. Low Temp. Phys. **107**, 93 (1997).

[5] D. Stauffer and A. L. Fetter, Phys. Rev. **168**, 156 (1968).

[6] E. V. Thuneberg, Phys. Rev. B **36**, 3583 (1987).

[7] P. Mathieu, B. Plaçais, and Y. Simon, Phys. Rev. B **29**, 2489 (1984).

[8] Ü. Parts *et al.*, Phys. Rev. Lett. **75**, 3320 (1995).

[9] J. M. Karimäki and E.V. Thuneberg (unpublished).

[10] E. B. Sonin, Physica B **210**, 234 (1995).

[11] H. K. Seppälä and G. E. Volovik, J. Low Temp. Phys. **51**, 279 (1983).